Int J Coal Sci Technol (2018) 5(3):315–327
https://doi.org/10.1007/s40789-018-0214-5

Study on the creep permeability of mining-cracked N_2 laterite as the key aquifuge for preserving water resources in Northwestern China

Wenping Li[1] · Qiqing Wang[1] · Shiliang Liu[1] · Yabing Pei[2]

Received: 19 September 2017 / Revised: 31 March 2018 / Accepted: 29 August 2018 / Published online: 6 September 2018

Abstract This research focused on the impact of mining on the permeability of key aquifuge (N_2 laterite) that is widespread in the arid and semi-arid areas of northwestern China and is critical for preserving water resources. The impact of mining stress recovery on the permeability of cracked N_2 laterite was assessed for parts of northwestern China that included the Jingle laterite and Baode laterite. The mineral compositions and swelling properties of the laterite at both locations were examined, and analytical results showed that the laterite contained abundant clay minerals. The Baode laterite exhibited higher expansibility than Jingle laterite. The triaxial creep permeability performance of laterite specimens with a prefabricated crack width of 1.0, 1.5, and 2.5 mm were tested. The results indicated that strain of cracked laterite all exhibited transient creep following each level of loading, and then unstable creep and stable creep. With the increase of loading, the transient creep deformation corresponding to each level of loading decreased, the unstable creep deformation produced by identical loading gradually and incrementally increased. The nonlinear power function equation was selected to fit creep grading curves which have high precision. The cracks within the laterite gradually closed with the stress recovery, and permeability gradually recovered. During the stress recovery, the narrower cracks exhibited a smaller change in permeability. However, for narrow cracks in mining soil, permeability recovered after mining stress when permeability was closer to initial permeability, and the Baode laterite showed greater recovery than that of the Jingle laterite.

Keywords Mining stress recovery · N_2 laterite · Mining crack · Permeability coefficient

1 Introduction

Coal occupies a dominant position in China's energy structure and is an important primary energy source for China. Coal resources account for about 70% of the nation's energy structure based on China's Development and Reform Commission (2012) (http://www.nea.gov.cn/), and in long-term forecasts, a Chinese coal-based energy structure will not be supplanted (Qiao et al. 2014). Because of the depletion of coal resources in the eastern mining area, coal resource development focus in China has quickly shifted to western China where the environment is more vulnerable. In 2013, coal production from the five northwestern provinces reached 17.9×10^8 t, accounting for 48% of national output. Future coal production in the western area will account for more than 70% of national coal output. The main coal seams in the western Jurassic coal fields are juxtaposed with a loose aquifer in the upper layer, clay aquifuge layer, bedrock, and a variety of other geologic characteristics, which typically results in five categories of geotechnical engineering conditions in area (Li et al. 2000), of which sand was the most common type of stratum. The strata featured a modern aeolian and Salawusu group sand layers with an underlying yellow clay and Neogene Pliocene laterite (N_2 laterite), and weathered

✉ Wenping Li
wpligroup@163.com

[1] School of Resources and Geosciences, China University of Mining and Technology, 1 University Road, Xuzhou 221116, Jiangsu, China

[2] Nuclear Industry Huzhou Engineering Surrey, Zhejiang 313000, Huzhou, China

bedrock and bedrock layers. The N_2 laterite is the regionally distributed strata that overlies the Jurassic coal seams in western China (Fig. 1) and is the primary aquifuge. The Salawusu group and the bedrock contained water, and bedrock group was a coal-containing strata that included mudstone, siltstone, and sandstone (Fig. 2). Since northwestern China is an arid and semi-arid region, and water is in shortage scarce resource, the ecological geotechnical environment is vulnerable. When the regional topography and ground conditions are suitable, shallow groundwater supplies are very valuable water resources, and have great significance for maintaining the ecological environment of the overall region (Xu et al. 2004; Li et al. 2017; Zhang et al. 2017). These are represented by the upper Pleistocene Salawusu group (Q_{3s}) sand aquifer which has a large distribution as the Maowusu desert beach, runoff water formed by rainfall at loess ravine region, lakes and reservoir water (Fig. 1). Coal mining in recent decades has resulted in a series of environmental issues in western China (Han et al. 1992; Fan and Jiang 2004; Yang et al. 2006; Miao 2008; Wang et al. 2008; Song 2009; Ma et al. 2010; Wang et al. 2011; Huang et al. 2012). The impact of coal mining on groundwater resources can be divided into three types (Wang et al. 2014; Qiao et al. 2017) including

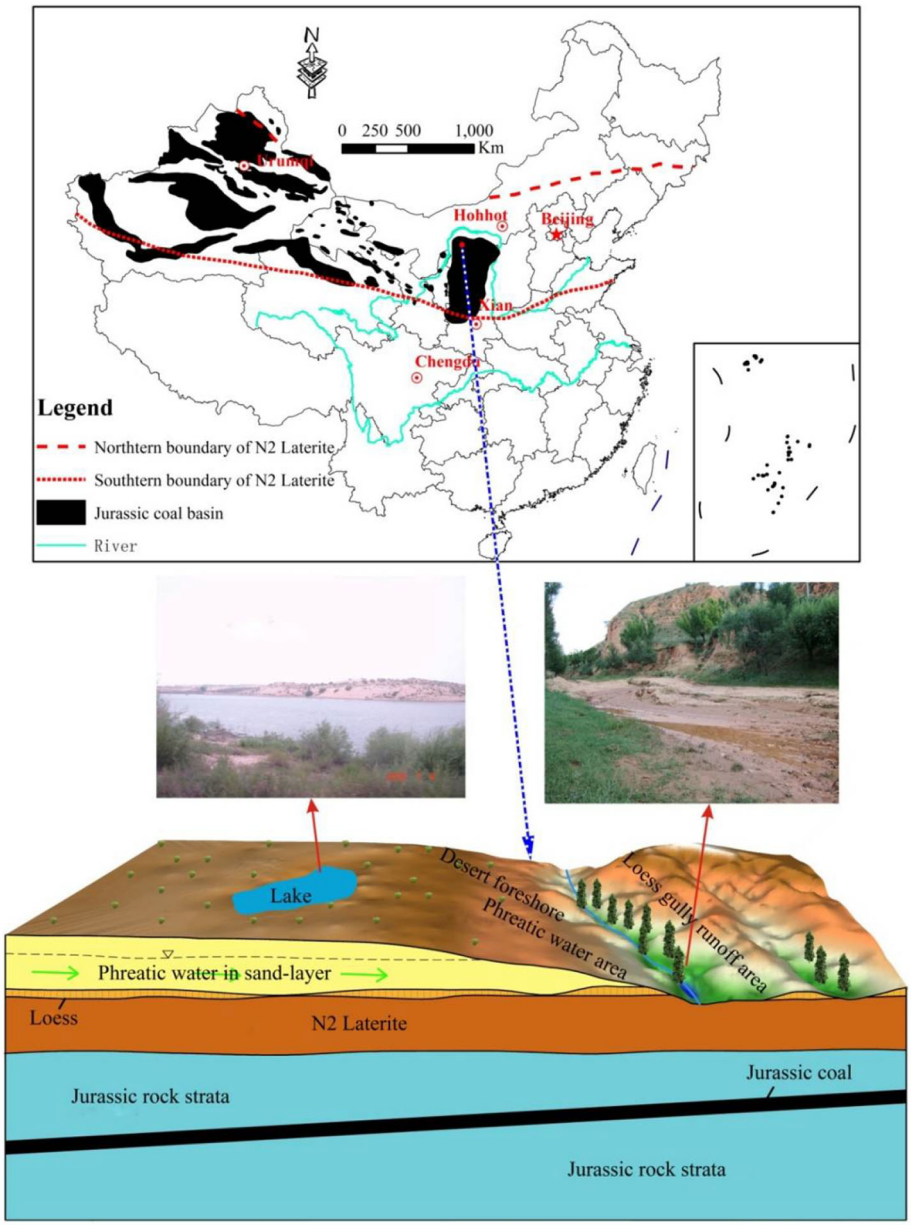

Fig. 1 Spatial relationship schematics for Chinese Jurassic coalfield distribution and Jurassic coal seams in research areas, as well as N_2 laterite aquifuge layer and shallow surface layer

Strata					Core columns	Thickness(m) Min~Max / Average	Cumulative depth(m)	Lithology characteristics
Erathem	System	Series	Formation	Member				
Cenozoic	Quaternary	Holocene				0~48.0 / 14.0	14.0	Dominated by aeolian sand including medium-fine sand and sandy soil, and alluvial-pluvial deposits among the valley beach and low-lying areas.
		Upper Pleistocene	Maolan Formation			0~15.0 / 8.0	22.0	Taupe fine sand and silt characterized by homogeneity and high porosity.
			Salawusu Formation			0~27.5 / 7.6	29.6	Dominated by silty sand and sandy clay, with gravel on the bottom layer.
		Middle Pleistocene	Lishi Formation			0~60.0 / 21.0	50.6	Ddominated by sandy clay, powder sand soil layer, paleosol layer, calcium nodule, with gravel on the bottom layer.
	Neogene	Pliocene	Baode Formation			0~107.8 / 30.5	81.1	Brownish red clay or sandy clay intercalated by calcium nodule and including vertebrate fossils.
Mesozoic	Jurassic	Middle Jurassic	Zhiluo Formation			0~101.2 / 25.0	106.1	Purple mudstone, sandstone, sandy mudstone, with glutenite on the bottom layer.
			Yan'an Formation	Fifth Member		0~25.8 / 12.0	120.1	2^{-2}th coal, offwhite medium or fine grained sandstone, intercalated by mudstone.
				Forth Member		0~52.5 / 40.0	160.1	3^{-1}th coal, 2th coal, lightgrey medium and fine grained sandstone intercalated by mudstone and sandstone.
				Third Member		0~68.5 / 45.0	205.1	4^{-2}th coal, offwhite medium grained arkose, fine-grained sandstone and sandy mudstone.
				Second Member		14.8~92.0 / 80.0	285.1	Grey or dark grey siltstone and 4th coal.
				First Member		7.4~60.0 / 26.4	311.5	5th coal and gray siltstone and fine-grained sandstone intercalated by medium grained sandstone and sandy mudstone.

Fig. 2 Comprehensive typical strata column for western coal field

(1) not influenced zone: coal seams are buried deeply; water flowing fractured zone does not develop to clay aquifuge layer (N_2 laterite layer) after mining, and coal mining almost has no impact on sand aquifer at the region with a thick development of clay aquifuge layer, and basically ground surface ecological environment is not affected; (2) zone of serious water leakage: coal seams are buried shallowly; water flowing fractured zone develops into sand aquifer and above, which results in quick loss of sand aquifer, water level rapidly decreases, and ground surface ecological environment severely deteriorates in a short time; (3) zone of general water leakage: after coal mining, water flowing fractured zone develops into clay aquifuge layer, where the clay aquifuge layer could lose a certain impermeability because of generated cracks, and later recovery of stress that leads to closure of the cracks in the clay and recovery of permeability to some extent. Water levels in the sand aquifer exhibited a significant decrease at the beginning of coal mining, and the ground surface ecological environment deteriorated. However, recovery of permeability from closure of the clay cracks allowed for water levels in sand aquifer to also recover, and ground surface ecological environment to be revitalized. Figure 3 shows a cross-sectional schematic for a typical mining operation in western China. The N_2 laterite over Jurassic coal layers distributed regionally in western China is of special natures. Most of current research on N_2 laterite is about its geologic components and engineering geology properties, and the research on the creep behavior and the permeability of N_2 laterite is hardly seen. At present, investigators have conducted numerous studies on common soil rheology and creep problems including experiments, soil creep modeling, and the numerical application of soil creep strain–stress model (Singh and Mitchell 1968; Garlanger 1972; Ladd 1977; Butterfield 1979; Mesri et al. 1981; Kabbaj et al. 1988; Zhan et al. 1993; Nash and Ryde 2001; Lan 2002; Chen et al. 2005, 2006; Yu et al. 2016). Experimental studies on mining stress recovery and creep permeability of special regional N_2 laterite are ongoing.

In this paper, stress recovery refers to the process of the cover stress re-establishment in the mined soil mass, which is gradually recovered to the self-weight stress of the overlying strata at the end of the mining process. This paper utilized double linkage triaxial testing machine for hydro-mechanical coupling in soft rock to conduct tri-axial creep permeability change testing on prefabricated N_2 laterite specimens (taken from Jingle laterite and Baode laterite from western Jingle County and Shenmu County, China, respectively). The research focused on the creep deformation and permeability change processes of N_2 laterite during mining stress recovery. The research outcomes can provide fundamental theory to predict the self-recovery of general water leakage zone which may occur within sand aquifers. In addition, the resulting data may

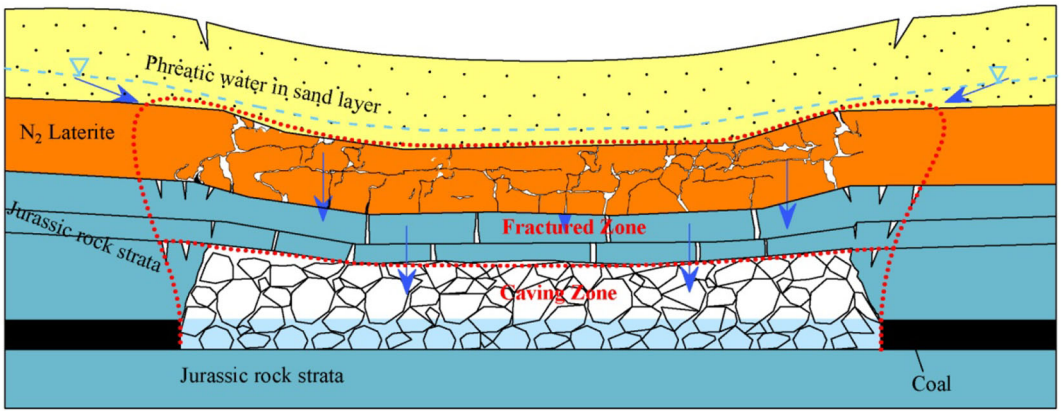

Fig. 3 Typical cross-sectional schematic for a western coal field mining operation

have significance for interpreting the process mechanisms of inflow reduction and leakage change after mining inrush occurs in western China.

2 Mineral composition and expansibility analysis of clay specimen

2.1 Clay mineral composition

There are a lot of factors influencing clay expansibility such as clay content, clay mineral type, organic matter content, and exchangeable citation group.

A D/Max-3B type of X-ray diffractometer was used to quantitatively analyze the clay mineral compositions of laterite specimens taken from two locations, and related testing results were shown in Fig. 4 and Table 1.

X-ray diffraction testing results showed that Jingle and Baode laterite contained abundant montmorillonite, kaolinite, illite, and clay minerals such as illite-montmorillonite mixture and chlorite. Montmorillonite comprised 23 and 21%, respectively, of the mixtures and was most influential on the permeability of clay. The mineral crystal structure of montmorillonite determined its high expansibility after water absorption. The water expansion characteristic of montmorillonite reduced the crack of clay, and accordingly resulted in a smaller permeability. In situ permeability test showed that cracks in Jingle laterite and Baode laterite did not develop under natural conditions, and after contact with water the montmorillonite minerals expanded to fill the internal cracks of soil and resulted in an aquifuge effect. However, after large-scale coal mining, a variety of cracks in soil would develop; corrosion would readily occur because of expansion of the clay layers, followed by a corresponding increase in permeability.

Mineral identification and molecular formula in Fig. 4 and Table 1 are as follows.

M—Montmoduonite: $(Na,Ca)_{0.7}$ $(Al,Mg)_4$ $(OH)_4$ $(SiAl)_8$ $O_{20}{\cdot}nH_2O$; I/M—Illite/Montmoduonite interstratified minerals; I—Illite: KAl_2 $(OH)_2$ $(AlSi)_4$ O_{10}; K—Kaolinite: Al_4 $(OH)_8$ Si_4 O_{10}; Cl—Chlorite: $(Mg,Fe,Al)_6$ $(OH)_8$ $(Si,Al)_4O_{10}$; Q—Quartz: SiO_2; C—Calcite: $CaCO_3$; F—Feldspar: (Na,Ca) $AlSi_3O_8$/(Na, K) $AlSi_3O_8$; C—Calcite: $CaCO_3$; O—Other(s).

2.2 Expansibility of clay

Expansibility is one of the important physical properties of clay. On the one hand, the porosity of clay deteriorates after clay absorbs water and expands making it relatively impermeable. On the other hand, the change of clay strain–stress field due to coal mining results in the partial rupture of clay, and the expansibility of clay regenerates the cracks in clay that can be accessible to water. The expansibility experiment of aquifuge clay is significant for understanding clay aquifuge layers in mining operations.

The indexes to characterize the expansibility of clay mainly include limited expansion (confined expansion), free expansion, and expansion force. The magnitude of limited expansion is mainly associated with compactness, natural moisture content and structural constitution of soil, but free expansion is the expansibility of clay without structural impact and represents the expansive tendency of clay; therefore, these two indexes were selected to evaluate the expansibility of N_2 laterite.

In this study, based on the "Standard for soil test method" (GB/T50123-1999), the loose, dry soil samples were prepared. The ratio of the volume increment to the original volume is calculated when the soil sample is stabilized in pure water. The free expansion ratio is based upon the formula as follows:

$$\delta_{ef} = \frac{V_{we} - V_0}{V_0} \times 100 \quad (1)$$

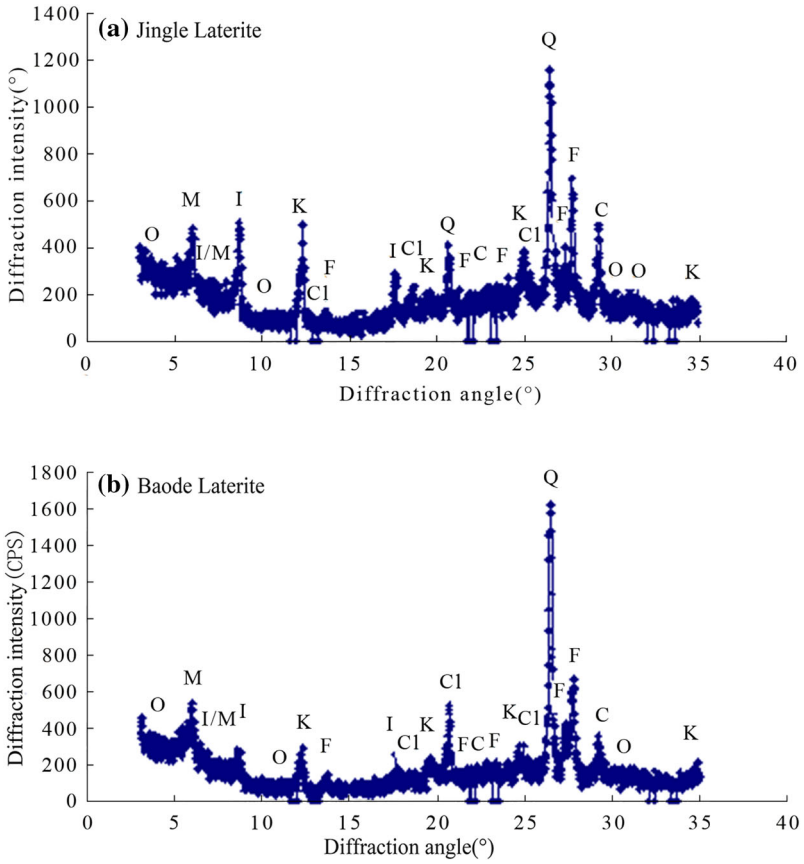

Fig. 4 X-ray diffraction spectrum of clay

Table 1 Relative quantitative analysis results of clay

No.	Name	Mineral composition (%)					
		M	I/M	I	K	Cl	O
1	Jingle laterite	24	15	25	23	11	2
2	Baode laterite	36	18	16	21	7	2

where, δ_{ef} is the free expansion ratio (%); V_{we} is the volume of the specimen in water; V_0 is the initial sample volume.

The confined expansion ratio test of N_2 laterite was based on the "Standard for soil test method" (GB/T50123-1999), Firstly, the prepared standard samples (diameter to height ratio of 1: 2) were dried and were placed into plastic bag. The gas in the plastic bag was discharged through the air pump so that the plastic bag was in close contact with the sample. And then, the sample volume was measured by drainage method. The specimens were wrapped with plastic film, and the amount of water was added according to the proportion. The specimens were placed in the steel mould with side limit. Finally, the axial deformation after confined expansion was tested by dial indicator. The confining expansion ratio was calculated by using Eq. (2):

$$\delta_e = \frac{z}{h_0} \times 100 \tag{2}$$

where, δ_e is the confining expansion ratio (%); z is the axial deformation after confined expansion; h_0 is the initial sample height.

In this study, confined expansion ratio and free expansion ratio were tested and the results were shown in Table 2. A difference in expansibility was documented between the Jingle laterite and the Baode laterite. Because of higher compactness and more expansive minerals, the Baode laterite exhibited better expansibility under confined conditions and better expansive tendency than those of the Jingle laterite.

3 Experimental design

3.1 Preparation of specimens

The undisturbed specimens of Jingle laterite and Baode laterite in this experiment were taken from Jingle County and the Shennan mining area of Shenmu County, western China. The sampling depth was 60–70 m for Jingle laterite,

Table 2 Expansive parameters of clay

No.	Name	Confining expansion ratio (%)	Free expansion ratio (%)
1	Jingle laterite	17.1	72.5
2	Jingle laterite	19.5	78.0
3	Jingle laterite	14.4	62.7
4	Baode laterite	17.8	74.9
5	Baode laterite	21.2	80.0
6	Baode laterite	16.8	70.3

and 70–85 m for Baode laterite. The basic mechanical properties of specimens were provided in Table 3.

In this experiment, specimens of cracked Jingle laterite and Baode laterite were used to simulate the cracked key clay aquifuge layer generated in the process of coal mining. The undisturbed soil samples were cut into the dimensions of φ38 mm × 76 mm. The initial cracks of the specimens were artificial, and a crack was located at the middle of the specimens. A total of six groups of cracked specimens were prepared with three groups of Jingle laterite and Baode laterite, respectively, having crack widths of 1.0, 1.5, or 2.5 mm, and crack lengths of 28 mm (Fig. 5).

3.2 Experimental equipment

Experimental instruments in this research included a double linkage tri-axial testing machine for hydro-mechanical coupling in soft rock that was jointly developed by the Institute of Rock and Soil Mechanics, Chinese Academy of Sciences, and the Changchun Chaoyang Experimental Factory. The rheometer is especially suitable to test the properties of soft rock and hard soil under various stress conditions. In addition to common functionalities of the tri-axial experimental machine, such as uniaxial and tri-axial compression experiment, the machine can also perform mechanical experiments of identical axial compression, different confining pressure, identical hydraulic pressure simultaneously for two specimens, confining pressure control, porous water pressure control, measure pore water pressure, and check the saturation degree of specimens.

Figure 6 shows the system theory for a dual linkage soft rock seepage-stress coupling triaxial rheometer. The instrument mainly consists of four components to achieve above functionalities including an axial loading part (primary machine), confining loading part (pressure chamber and loading unit), pore water loading part, and control part (computer and controller). A pad was used to uniformly transfer force between the upper and lower tri-axial pressure chambers.

3.3 Experimental methodology and procedure

In order to more closely reflect the actual situation during experiments, the experimental soil specimens were initially saturated. Three-isometric hydrostatic pressures ($\sigma_1 = \sigma_2 = \sigma_3 = 0.2$ MPa) (in situ horizontal effective stress) were applied, in the process of saturation, at the two ends of specimens to provide backpressure for saturation and to avoid disturbance against specimens. At first, isotropic pressures were increased to 0.2 MPa with a loading rate of 0.139 kPa/min, then a backpressure of 0.1 MPa was applied at the top and bottom of specimens, which was maintained for 24 h. Saturation status was judged by checking the variation of pore pressure coefficient B, and when Skempton B coefficient reached 0.85, the specimens were regarded as saturated. The burial depth of laterite

Table 3 Basic mechanical properties of clay aquifuge

Name	Moisture content (%)	Density (g/cm^3)	Specific gravity	Void ratio	Cohesion (kPa)	Internal friction angle (°)	Compressibility (MPa^{-1})	Compression modulus (MPa)	Unconfined compressive strength (kPa)
Jingle laterite	9.1–20.8	1.75–2.11	2.69–2.71	0.47–0.76	38–101	27.9–33.8	0.06–0.11	7–22.1	119–159
Baode laterite	14.5–26.5	1.80–2.05	2.70–2.73	0.57–0.92	76–96	28.2–32.9	0.08–0.25	15.5–28.3	182–212

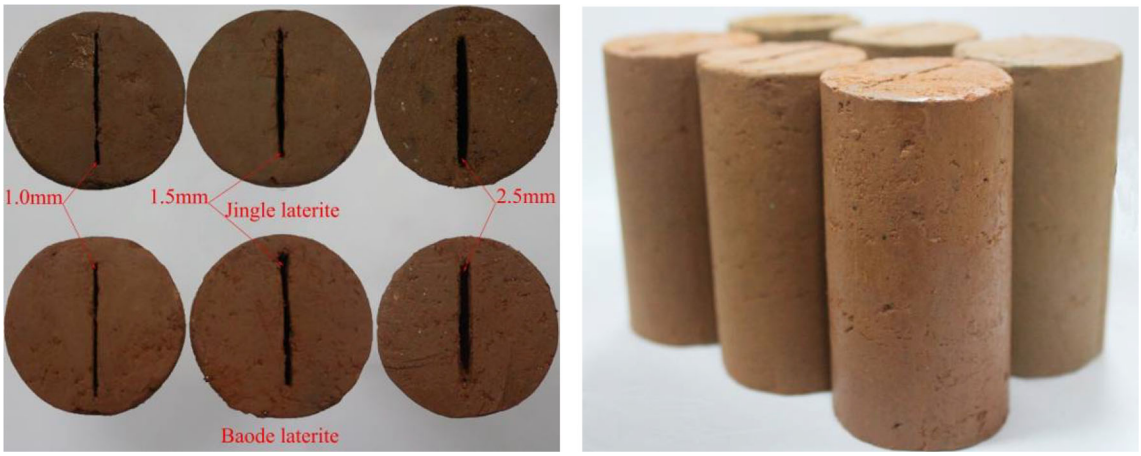

Fig. 5 Soil specimen

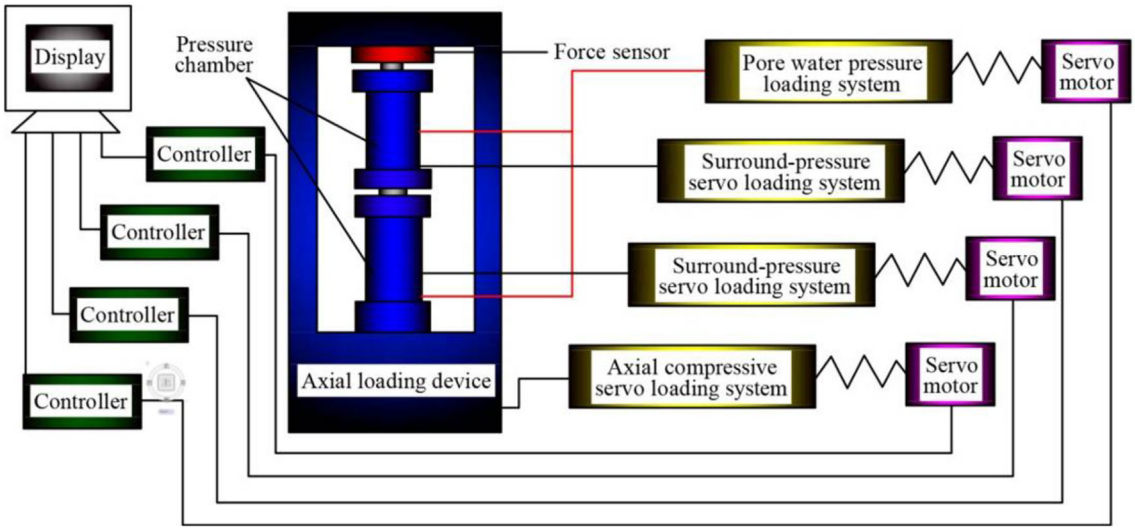

Fig. 6 Schematic diagram of double linkage tri-axial testing machine for hydro-mechanical coupling in soft rock

ranges from 0 to 225 m, so the maximum of loads is about 4.5 MPa. In this study, experimental soil specimens were loaded in various loads of 1.5 MPa, 2.5 MPa, 3.5 MPa, and 4.5 MPa as shown in Fig. 7. Each loading was maintained for about one day. After deformation of specimens stabilized, a steady state method was used to test their permeability coefficients under the condition of keeping confining pressure and axial pressure constant (the steady state method referred to application of a hydrostatic pressure of 0.2 MPa on the top of specimen. The amount of water effluent at the bottom of the specimen was measured using a high precision soap-bubble flowmeter, and the permeability coefficient was calculated after the effluent stabilized before applying the next loading. Stress and deformation were monitored during implementation of experiments.

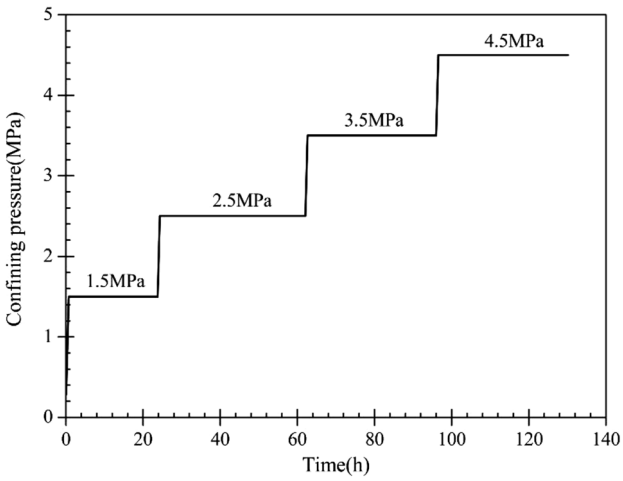

Fig. 7 Loading time history curve of soil specimen

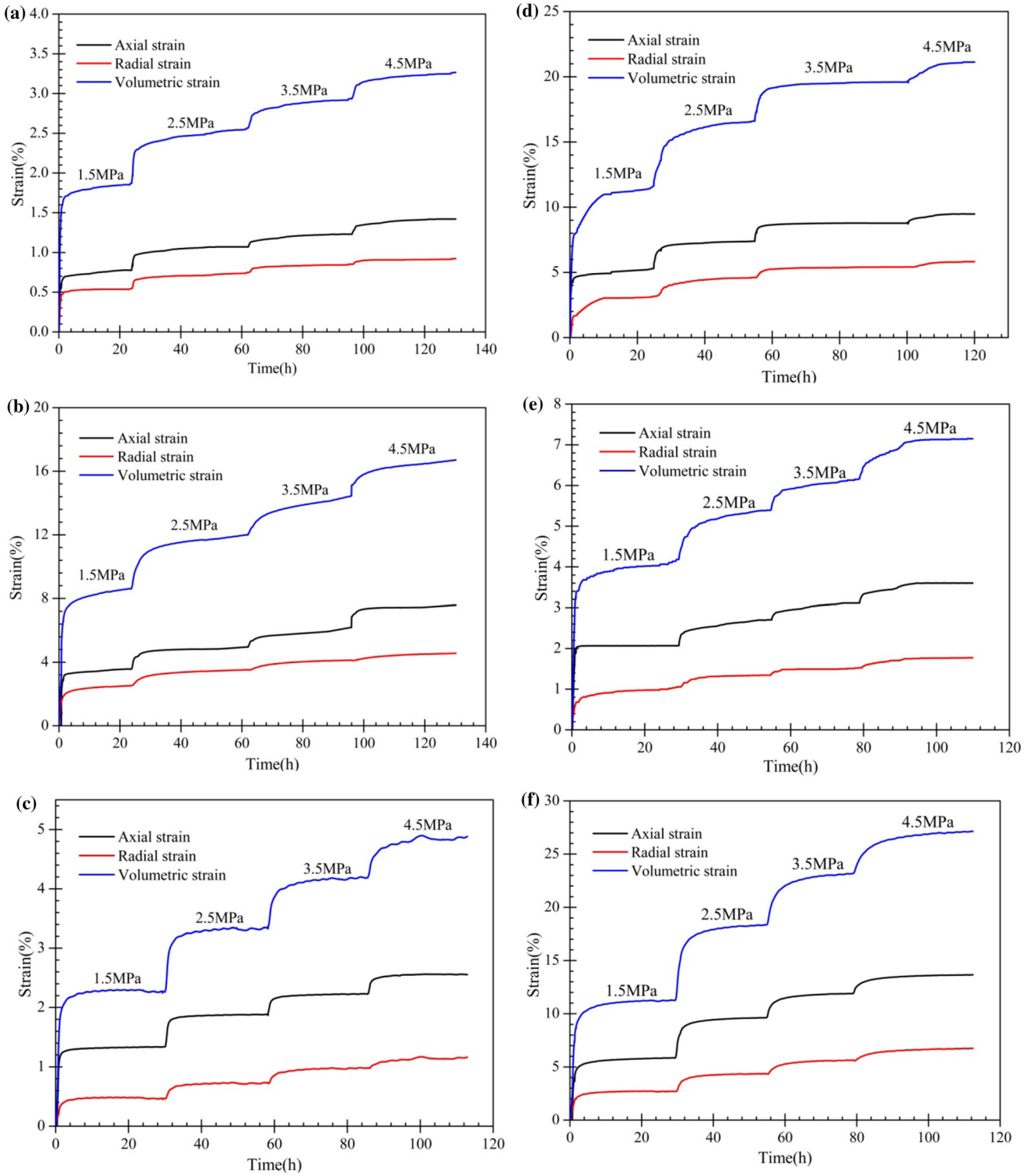

Fig. 8 Creep testing curves under different stress levels: **a** Jingle laterite specimens with 1.0 mm wide cracks, **b** Baode laterite specimens with 1.0 mm wide cracks, **c** Jingle laterite specimens with 1.5 mm wide cracks, **d** Baode laterite specimens with 1.5 mm wide cracks, **e** Jingle laterite specimens with 2.5 mm wide cracks, **f** Baode laterite specimens with 2.5 mm wide cracks

Table 4 Creep parameters under different loads

Laterite specimens (crack width)	Loading stage	σ	A	m	n	R^2
Jingle (1.0 mm)	1	1.5	2.57058	− 1.46048	0.09449	0.6387
	2	2.5	0.44476	− 0.35958	0.21188	0.91405
	3	3.5	0.18009	− 0.26602	0.29904	0.95304
	4	4.5	0.17139	− 0.13105	0.2387	0.92984
Baode (1.0 mm)	1	1.5	7.06889	− 0.71559	0.16912	0.74458
	2	2.5	3.36961	− 1.03797	0.26813	0.92879
	3	3.5	1.23546	− 0.63005	0.41189	0.98517
	4	4.5	0.88581	0.04824	0.24245	0.98573
Jingle (1.5 mm)	1	1.5	2.85433	− 1.2774	0.10414	0.51142
	2	2.5	1.12045	− 0.55521	0.15635	0.72924
	3	3.5	0.62648	− 0.32103	0.2241	0.8602
	4	4.5	0.81095	− 0.66556	0.27499	0.87651
Baode (1.5 mm)	1	1.5	11.51706	− 1.15144	0.16189	0.8662
	2	2.5	4.13109	− 0.79908	0.28631	0.91062
	3	3.5	2.75267	− 0.38968	0.16826	0.81978
	4	4.5	1.05204	− 0.62458	0.47039	0.90209
Jingle (2.5 mm)	1	1.5	3.55611	− 0.45399	0.10699	0.66572
	2	2.5	0.65894	− 0.39736	0.31271	0.95953
	3	3.5	0.45942	− 0.36575	0.29258	0.98015
	4	4.5	0.70362	− 0.46219	0.32506	0.90784
Baode (2.5 mm)	1	1.5	3.46662	1.80396	0.149	0.66265
	2	2.5	4.555	− 0.29966	0.2392	0.85253
	3	3.5	2.96932	− 0.3596	0.31033	0.90712
	4	4.5	2.38043	− 0.37523	0.31802	0.92733

4 Results and discussion

Creep testing curves under different stress levels for Jingle laterite and Baode laterite with crack widths of 1.0, 1.5 and 2.5 mm were shown in Fig. 8. The figure showed that the specimens for both locations exhibited transient creep following each level of loading, and then unstable creep and stable creep. With the increase of loading, the transient creep deformation corresponding to each level of loading decreased, the unstable creep deformation produced by identical loading gradually and incrementally increased. This meant that mining cracked N_2 laterite had a larger deformation at the beginning of stress recovery, i.e. closing of crack was more apparent; but the later deformation was smaller and smaller until it became stable. In addition, under the application of identical loads, a larger crack width occurred for identical soil specimens and there was greater transient creep deformation. This indicated that a larger mining crack width during soil stress recovery. Under application of identical loading and with the same crack width, the Baode laterite exhibited greater deformation than Jingle laterite. This was mainly because of the differences in mechanical properties. On the one hand, the Baode laterite contained abundant clay minerals. On the other hand, the void ratio of Baode laterite was larger than that of Jingle laterite. Therefore, the Baode laterite was more condensable than Jingle laterite under equivalent conditions.

The creep testing curves under different stress levels show that the creep process of cracked N_2 laterite presents nonlinear characteristics. In this study, the nonlinear power function creep model was used to describe the creep behavior of cracked N_2 laterite in three axis creep test. The model can be expressed by the given formula equation.

$$\varepsilon = A\sigma^m t^n \tag{3}$$

where, ε is creep strain; A, m and n are coefficients to be determined; σ is loading confining pressure; and t is reference time.

Polynomial regression analysis method was used to fit empirical equation, which got corresponding parameters of each specimen under different stress levels (Table 4). From Table 4, it was seen that the fitting curves agreed well with experimental results when the applied loads are at high levels (2.5 MPa, 3.5 MPa, 4.5 MPa). However, the fitting

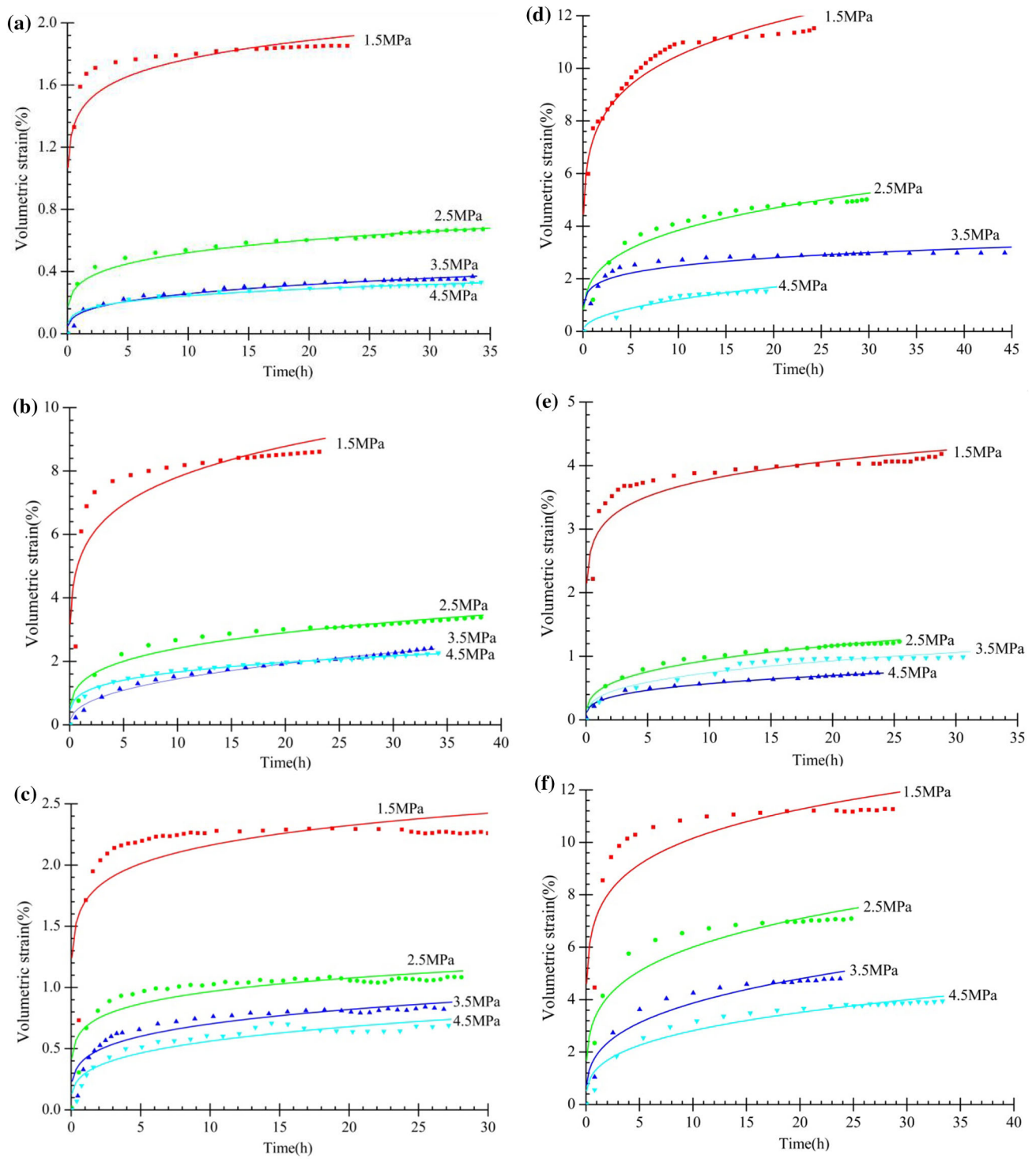

Fig. 9 Creep test results and fitting curves under different levels of loading: **a** Jingle laterite specimens with 1.0 mm wide cracks, **b** Baode laterite specimens with 1.0 mm wide cracks, **c** Jingle laterite specimens with 1.5 mm wide cracks, **d** Baode laterite specimens with 1.5 mm wide cracks, **e** Jingle laterite specimens with 2.5 mm wide cracks, **f** Baode laterite specimens with 2.5 mm wide cracks

curve showed large difference with experimental results. The most important reason is that the closure degree of the cracks within the laterite is bigger when the applied load is 1.5 MPa. In general, the correlation coefficients (R^2) of most of the fitting results were greater than 0.9, which showed that the fitting precision is very high. The change of creep deformation of cracked N_2 laterite with time can be well reflected by using this nonlinear power function

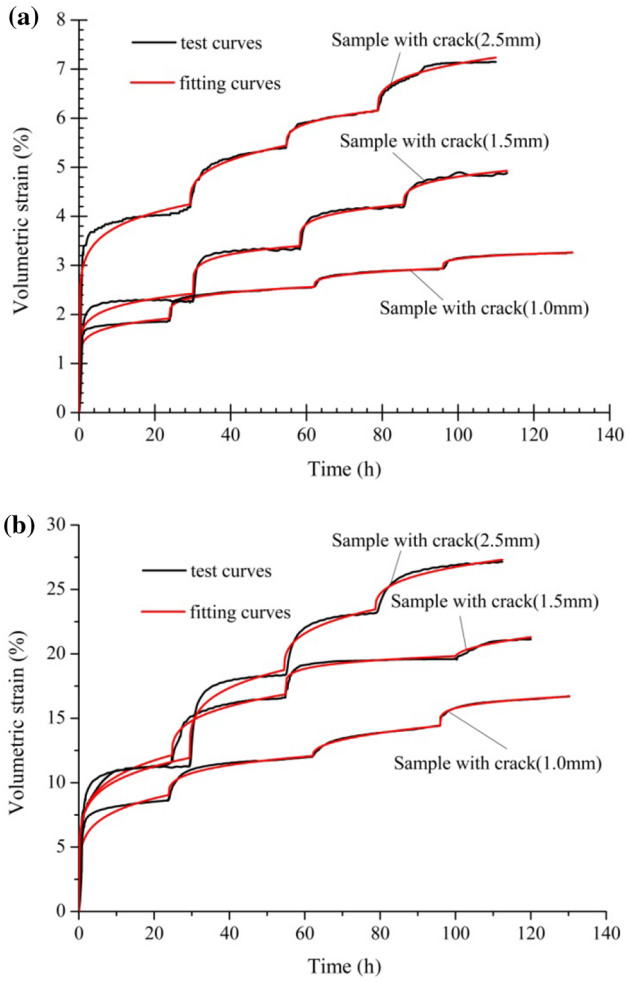

Fig. 10 Creep test results and fitting curves of model: **a** Jingle laterite specimens, **b** Baode laterite specimens

creep model. Based on empirical equation of polynomial regression fitting, creep grading curves of cracked N_2 laterite in several load conditions were obtained as shown in Fig. 9. The creep test results and fitting curves of model for Jingle and Baode laterite specimens were shown in Fig. 10.

The relationship between the permeability and confining pressure of cracked N_2 laterites at two locations were presented in Fig. 11. Figure 11 showed that there was an exponential relationship between permeability and confining pressure of cracked N_2 laterites that can be approximately described by Eq. (4).

$$K = K_0 e^{-\lambda\sigma} \tag{4}$$

where, K is permeability coefficient; K_0 and λ are coefficients to be determined; and σ is loading confining pressure. Table 5 showed that the corresponding values of K_0 and λ for different conditions.

The experimental and fitting results showed that the permeability coefficients of cracked Jingle and Baode

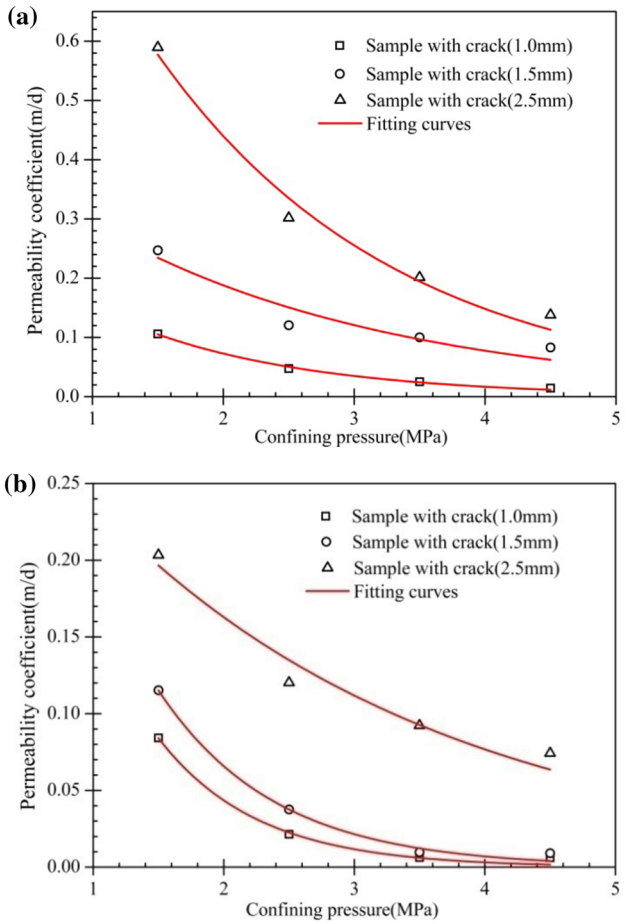

Fig. 11 Relationship curves of permeability coefficient and confining pressure: **a** Jingle laterite, **b** Baode laterite

Table 5 Fitting parameters of the relationship between the permeability and confining pressure

Laterite specimens(crack width)	K_0	λ	R^2
Jingle (1.0 mm)	0.6044	1.3154	0.9922
Jingle (1.5 mm)	0.6177	1.1198	0.9937
Jingle (2.5 mm)	0.3457	0.3763	0.9422
Baode (1.0 mm)	0.3158	0.7336	0.9944
Baode (1.5 mm)	0.4553	0.4423	0.8636
Baode (2.5 mm)	1.3054	0.5439	0.9755

laterites gradually decreased with the increase of loading, and the decrease in magnitude of the permeability coefficient was gradual under the application of identical loading. This indicated that the mining cracked laterite had a higher variation of permeability at the beginning of stress recovery, i.e. the extent of crack closure was more evident; but the variation of permeability gradually stabilized because deformation was minimized. In addition, in similar soil specimens, larger crack widths corresponded to larger

variations of permeability during stress recovery. When stress completely recovered, the soil specimens with larger crack widths exhibited larger permeability coefficients. This indicated that smaller mining soil crack widths resulted in smaller permeability coefficients after stress recovery, and larger crack widths resulted in more severe soil damage and limited permeability recovery.

Under the application of identical loading for soil specimens with similar crack widths, the permeability coefficient of Baode laterite was about less than one-third of Jingle laterite. The permeability of mining cracked Baode laterite was slightly higher than that of Jingle laterite after mining recovery. The reason for this is that engineering geological properties of the laterite at both locations are different. The Baode laterite contained richer clay minerals and exhibited higher expansibility than Jingle laterite.

5 Conclusion

(1) Through analyzing the mineral compositions and expansibility of Jingle laterite and Baode laterite, this research shows that both Jingle laterite and Baode laterite contained abundant montmorillonite, kaolinite, and illite, as well as some clay materials such illite-montmorillonite and chlorite. Montmorillonite comprised 23 and 21%, and was the most abundant mineral. Jingle laterite and Baode laterite exhibited differences in expansibility. Baode laterite had a higher expansibility than Jingle laterite under confining conditions because it was more compact and was comprised of more expansive minerals.

(2) Specimens for Jingle laterite and Baode laterite exhibited transient creep following each level of loading, and then unstable creep and stable creep. With the increase of loading, the transient creep deformation corresponding to each level of loading decreased, the unstable creep deformation produced by identical loading gradually and incrementally increased. The nonlinear power function equation was selected to fit creep grading curves which have high precision.

(3) Mining cracks in Jingle laterite and Baode laterite were gradually closed and permeability recovered following the recovery of mining stress. In the process of stress recovery, smaller crack widths and lower variations in permeability were observed; however, permeability was closer to the initial permeability in specimens that had smaller soil cracks after recovery of mining stress. Baode laterite with mining cracks exhibited higher recovery ability than that of Jingle laterite.

Acknowledgements The authors express their gratitude to everyone that provided assistance for the present study. The study was jointly supported by the State Key Program of National Natural Science Foundation of China (Grant No. 41430643) and the National Key Basic Research Program of China (973 Program) (Grant No. 2015CB251601).

References

Butterfield R (1979) A natural compression law for soils. Géotechnique 29(4):469–480

Chen X, Zhu H, Zhang F, Zhang B (2005) Experimental study on time-dependent deformation of soft soil. Chin J Rock Mechan Eng 24(12):2142–2148 **(in Chinese)**

Chen W, Wu G, Dai Y (2006) Stability analysis of abandoned salt caverns used for underground gas storage. Chin J Rock Mechan Eng 25(4):848–854 **(in Chinese)**

Fan L, Jiang Z (2004) Engineering geologic background of coal mining under water-containing condition in Yushen coal mining area. Coal Geol Explor 32(5):32–35 **(in Chinese)**

Garlanger JE (1972) The consolidation of soils exhibiting creep under constant effective stress. Geotechnique 22(1):71–78

GB/T50123-1999 (1999) Standard for soil test method, pp 127–130 **(in chinese)**

Han S, Fan L, Yang B (1992) Exploitation of north Shaanxi Jurassic coal field hydrogeologic and engineering geological problems for analysis. Coal Geol China 4(1):49–52 **(in Chinese)**

Huang H, Wang C, Bai H, Wang Z (2012) Water protection in the western semiarid coal mining regions of China: a case study. Int J Min Sci Technol 22(5):719–723

Kabbaj M, Tavenas F, Leroueil S (1988) In situ and laboratory stress–strain relationships. Geotechnique 38(1):83–100

Ladd CC (1977) Stress-deformation and strength characteristics, state of the art report. In Proceedings of 9th ISFMFE 4, pp 421–494

Lan L (2002) Studies on the non-linear rheologic consolidation behavior of layered soft clayey soils. (Doctoral dissertation, Zhejiang University) **(in Chinese)**

Li W, Ye G, Zhang L, Duan Z, Zhai L (2000) Study on the engineering geological condition of protected water resources during coal mining action in Yushenfu mine area in the north Shaanxi provice. J China Coal Soc 25(5):449–454 **(in Chinese)**

Li W, Wang Q, Li X (2017) Reconstruction of aquifuge: the engineering geological study of N_2 laterite located in key aquifuge concerning coal mining with water protection in northwest China. J China Coal Soc 42(1):88–97 **(in Chinese)**

Ma X, Wang W, Fan L, Yang Z, Zhu L (2010) Coal mining impacting on springs in ecologically fragile mining area. Coal Geol China 22(1):32–36 **(in Chinese)**

Mesri G, Febres-Cordero E, Shields D, Castro A (1981) Shear stress-strain-time behaviour of clays. Geotechnique 31(4):537–552

Miao L (2008) Study on hosting pattern and influence of the seam exploitation on water resources in the main seam of Yushenfu deposit. (Doctoral dissertation, Xi'an: Xi'an University of Science and Technology) **(in Chinese)**

Nash DFT, Ryde SJ (2001) Modelling consolidation accelerated by vertical drains in soils subject to creep. Géotechnique 51(3):257–273

Qiao W, Li W, Zhang X (2014) Characteristic of water chemistry and hydrodynamics of deep karst and its influence on deep coal mining. Arab J Geosci 7(4):1261–1275

Qiao W, Li W, Li T, Chang J, Wang Q (2017) Effects of coal mining on shallow water resources in semiarid regions: a case study in the Shennan mining area, Shaanxi, China. Mine Water Environ 36(1):104–113

Singh A, Mitchell JK (1968) General stress-strain-time function for soils. J Soil Mech Found Div 94(1):21–46

Song S (2009) The quantitative evaluation of eco-environment damage induced by coal exploitation in Yushenfu mining area. (Doctoral dissertation, Xi'an: Xi'an University of Science and Technology) **(in Chinese)**

Wang L, Wei S, Wang Q (2008) Effect of coal exploitation on groundwater and vegetation in the Yushenfu Coal Mine. J China Coal Soc 33(12):1408–1414 **(in Chinese)**

Wang S, Fan L, Ma X (2011) The coal mining and ecological water-level protection. China Min Mag 19(ZK): 212–216 **(in Chinese)**

Wang Q, Li W, Li T (2014) Division types of geological conditions at mining with water protection in ecological fragile area of northern Shaanxi. J Eng Geol 22(3):515–521 **(in Chinese)**

Xu JL, Zhu WB, Lai WQ, Qian MG (2004) Green mining techniques in the coal mines of China. J Mines Metals Fuels 52(12):395–398

Yang Z, Wang W, Huang J, Duan L (2006) Research on buried depth of eco-safety about groundwater table in the blown-sand region of the Northern Shaanxi Province. J Northwest A&F Univ 34(8):67–74 **(in Chinese)**

Yu M, Mao X, Hu X (2016) Shear creep characteristics and constitutive model of limestone. Int J Min Sci Technol 26(3):423–428

Zhan M, Qian J, Chen X (1993) Test on rheological behavior of soft soil and rheologic model. Chin J Geotech Eng 15(3):54–62 **(in Chinese)**

Zhang D, Li W, Lai X, Fan G, Liu W (2017) Development on basic theory of water protection during coal mining in northwest of China. J China Coal Soc 42(1):36–43 **(in Chinese)**